Seismic performance of small earth dams with sloping core zones and geosynthetic clay liners using full-scale shaking table tests

Sawada, Yutaka ; Nakazawa, Hiroshi ; Oda, Tetsuya ; Kobayashi, Seita ; Shibuya, Satoru ; Kawabata, Toshinori

(Citation)
Soils and Foundations,58(3):519-533

(Issue Date)
2018-06

(Resource Type)
journal article

(Version)
Version of Record

HOSTED BY
ELSEVIER
Available online at www.sciencedirect.com
ScienceDirect
Soils and Foundations 58 (2018) 519–533
SOILS AND FOUNDATIONS
www.elsevier.com/locate/sandf

Seismic performance of small earth dams with sloping core zones and geosynthetic clay liners using full-scale shaking table tests

Yutaka Sawada [a,*], Hiroshi Nakazawa [b], Tetsuya Oda [c], Seita Kobayashi [c], Satoru Shibuya [d], Toshinori Kawabata [a]

[a] *Graduate School of Agricultural Science, Kobe University, Japan*
[b] *National Research Institute for Earth Science and Disaster Resilience, Japan*
[c] *Hyogo Prefecture, Japan*
[d] *Graduate School of Engineering, Kobe University, Japan*

Received 7 December 2016; received in revised form 7 September 2017; accepted 29 January 2018
Available online 25 June 2018

Abstract

In Japan, a large number of old small earth dams are in critical need of repair due to leakage and poor earthquake resistance. In addition to cohesive soils, geosynthetic clay liners (GCLs) are used as impervious materials to repair such dams. This paper discusses the seismic performance of small earth dams, with reservoirs on their upstream side, repaired with a sloping core zone and a GCL on the basis of the results of full-scale shaking table tests performed at the E-Defense facility. The main focus is on the differences in mechanical behavior between the upstream and downstream sides of the dam. The results elucidate that the effective stress of the upstream embankment materials increased because of the undrained shear behavior of the compacted soils, although the deformation on the upstream side was larger than that on the downstream side. A large phase difference in the measured accelerations between the upstream slope and the downstream slope was also observed. Therefore, it is concluded that significant differences occurred in the dynamic behavior of the upstream side and the downstream side.

Keywords: Small earth dam; Full-scale shaking table test; Geosynthetic clay liner; Residual deformation; Excess pore water pressure

1. Introduction

There are approximately 200,000 small earth dams in Japan. Among them, around 70% were constructed more than 150 years ago and have experienced significant deterioration (Ministry of Agriculture, Forestry and Fisheries, 2017). Since these dams were constructed without modern compaction machines and techniques, their embankment stabilities are unclear. Furthermore, it is possible that a strong earthquake will occur along the Nankai Trough sometime in the next 30 years. Thus, in regions where the possibility of a strong earthquake is high, it is important to increase the earthquake resistance of the small earth dams.

In the standard method for improving small, deteriorated earth dams, a sloping core zone is built on the upstream side of the dam using cohesive soils as the impermeable materials. However, in recent years, the supply of high-quality impermeable materials at dam sites has been exhausted, and it is difficult to bring in embankment materials using dump trucks because of narrow roads. For sites where it is difficult to obtain embankment materials, small earth dams may be improved with impervious materials such as rubber membranes and synthetic resin sheets

Peer review under responsibility of The Japanese Geotechnical Society.
* Corresponding author.
E-mail address: sawa@harbor.kobe-u.ac.jp (Y. Sawada).

https://doi.org/10.1016/j.sandf.2018.01.003
0038-0806/

(Ministry of Agriculture, Forestry and Fisheries, 2015a). Geosynthetic clay liners (GCLs), which have been used at waste disposal sites, have also been adopted in recent years for the repair of small earth dams (e.g., Aoyama, 2011). However, the seismic performance of small earth dams with GCLs has not been examined, and no design guidelines for small earth dams with GCLs have been established.

With respect to earthquake damage to small earth dams, Tani and Hasegawa (1987) described the causes and modes of failure on the basis of damage survey reports on five past earthquakes, including the 1983 Japan Sea Chubu Earthquake. They reported that (1) slide failure and the lateral deformation of embankments occur approximately twice as often on the upstream side of a dam as on the downstream side; (2) the damage ratio by earthquakes is high when the foundation or embankment consists of sandy soils; and (3) serious damage, such as breaches, tends to occur when the water level is high.

With respect to earthquake damage during the past twenty years, Tani (1996) reported the features and mechanism of the damage caused by the 1995 Hyogo-ken Nanbu Earthquake. This earthquake damaged 1222 small earth dams, many of which were located within a radius of 30 km from the epicenter. The damage to some of these dams may have been caused by liquefaction. The 2011 Off-the-Pacific-Coast-of-Tohoku Earthquake damaged 750 of the 3730 small earth dams in Fukushima Prefecture via modes including slide failure and the lateral deformation of embankments (Hori et al., 2012; Mohri et al., 2014). The Fujinuma, Aotashin, and Naka Dams experienced breaches and, in particular, the breach of the Fujinuma Dam (18.5 m in height) caused severe damage to houses located downstream of the dam. According to a report put out by Fukushima Prefecture (2011), the sliding failure occurred toward the upstream side of the dam because of the decline in strength of the embankment materials, comprising highly saturated sandy soils, and due to the long period of strong ground motion. The water stored in the dam, which was full when the earthquake occurred, overflowed and breached the dam embankment.

Several researchers have examined the seismic behavior of dam embankments using physical models and numerical analyses (e.g., Hasegawa and Kikusawa, 1981; Ohne et al., 1983). Many of these studies involved the investigation of the failure process of earth dams without reservoirs. The seismic performance of earth-fill dams with reservoirs of water have also been examined by some researchers (e.g., Kim et al., 2011; Yuan et al., 2014; Kawai et al., 2015). Sendir et al. (2010) showed that the deformation of a dam body increases with decreasing relative soil density. Even though the slope was gentler at the upstream side of the dam in Sendir et al., they found that the deformation was greater on the upstream side of the dam than on the downstream side. However, the seismic behavior of embankments with sloping core zones and GCLs has only been examined in a few small-scale modeling studies (Koyama et al., 2014; Jeong et al., 2016).

To examine the seismic behavior of small earth dams that have been repaired with sloping core zones or GCLs, the authors conducted full-scale shaking table tests on two embankments as high as 3 m, as shown in Fig. 1 (Sawada et al., 2016). One embankment had a sloping core zone and the other had a GCL. When the embankments were subjected to shaking corresponding to Level-2 seismic motion, as defined in the Japanese guidelines for the seismic design of agricultural facilities (Ministry of Agriculture, Forestry and Fisheries, 2015b), large longitudinal cracks were seen to develop at the crest of the embankment containing a GCL, although no water leakage was observed in either case. Observations of embankment cross-sections by Oda et al. (2016) have revealed that the presence of a GCL can cause the development of cracks. In addition, data on the recorded accelerations around a GCL have shown that the seismic characteristics at the upstream side separated by the GCL differed from those at the downstream side. Nakazawa et al. (2017) applied three-dimensional terrestrial laser measurements to reveal the location and characteristics of cracks at the crest of an embankment with a GCL and clarified its effectiveness. However, the recorded accelerations and response pore water pressure throughout the entire embankment were not discussed in their studies and many details of the seismic behavior have not yet been clarified.

In this study, to examine the performance of small earth dams and to provide a benchmark for numerical simulations, the deformation, acceleration, and pore water pressure measured in full-scale shaking table tests are discussed. In particular, the differences in dynamic behavior between the upstream and downstream sides of the dam are addressed.

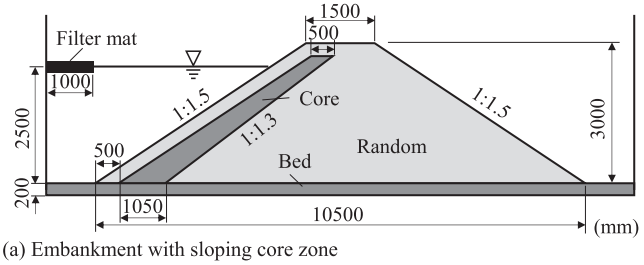

(a) Embankment with sloping core zone

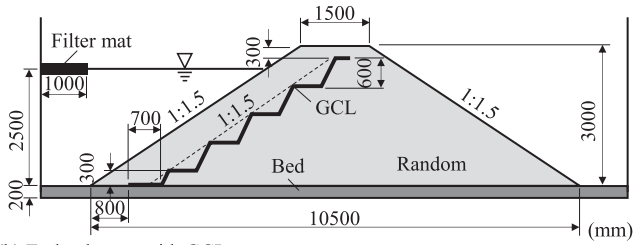

(b) Embankment with GCL

Fig. 1. Model configurations (modified from Sawada et al., 2016).

2. Experimental setup

2.1. Shaking table

This study was carried out using the three-dimensional, full-scale earthquake testing facility of the National Research Institute for Earth Science and Disaster Resilience, which is widely known as E-Defense (Tabata et al., 2017). The shaking table has the dimensions of 15 m × 20 m, and the payload is 1200 t. The maximum accelerations at the maximum loading are 900 cm/s^2 in the horizontal direction and 1500 cm/s^2 in the vertical direction. The maximum displacements are ±100 cm in the horizontal direction and ±50 cm in the vertical direction. The facility can simulate earthquake failures for full-scale models of various kinds of structures and buildings

2.2. Soil containers

In this study, steel containers (length = 12.59 m, height = 3.55 m, width = 2.50 m, and weight = 105 t) were designed and used. As shown in Photo 1, two containers were placed side-by-side on the shaking table. H-section steel beams were placed on top of the soil containers to reinforce the containers and to provide a location for the installation of the instruments. In addition, a filter mat was installed on the water surface to dissipate the wave energy, and the upstream part of the container was covered with a vinyl sheet to prevent the outflow of water.

2.3. Model configurations

Fig. 1 shows the model configurations for the two types of embankment models. The models were constructed in the above-described steel containers and were tested simultaneously. One model was an embankment with a sloping core zone (hereinafter referred to as "ESCZ") and the other was an embankment with a GCL (hereinafter referred to as "EGCL"). The bed width and thickness were 12.59 and 0.2 m, respectively. The width of the crest of both embankments was 1.5 m and the height was 3.0 m. The inclination of the embankments was 1:1.5 as per the Japanese guidelines (Ministry of Agriculture, Forestry and Fisheries, 2015a). There was a reservoir on the upstream side of each embankment.

2.4. Soil materials and GCL

2.4.1. Core material

In the present study, cohesive soil with gravel, excavated from a borrow-pit in Ono City, Hyogo Prefecture, was used as the core material at the upstream slope of the embankment, as shown in Fig. 1. According to the Unified Soil Classification System of Japan, the soil is classified as GFS. The material properties, the grain size cumulative curves, and the compaction curves are shown in Table 1, Figs. 2 and 3, respectively. Permeability tests were performed using two kinds of specimens with maximum particle diameters of 2 and 19 mm. The permeability coefficient of the 19-mm-diameter specimen was found to be 10 times higher than that of the 2-mm-diameter specimen. Since the grain size distribution was different for each case, the fine contents were also different. Moreover, the skeleton structures of the soil after compaction were also likely to

Table 1
Properties of the core material.

Soil particle density ρ_s (g/cm^3)	2.648
Average diameter D_{50} (mm)	1.0
Uniformity coefficient U_C	1000
Coefficient of curvature U_C'	1.6
Optimum water content w_{opt} (%)	15.7
Maximum dry density ρ_{dmax} (g/cm^3)	1.824
Coefficient of permeability (D_{max} = 2mm, D = 90%) k (m/s)	6.80 × 10^{-7}
Coefficient of permeability (D_{max} = 19mm, D = 90%) k (m/s)	9.42 × 10^{-6}
Liquid limit w_L (%)	33.1
Plastic limit w_P (%)	21.5

Photo 1. Shaking table and soil containers (Sawada et al., 2016).

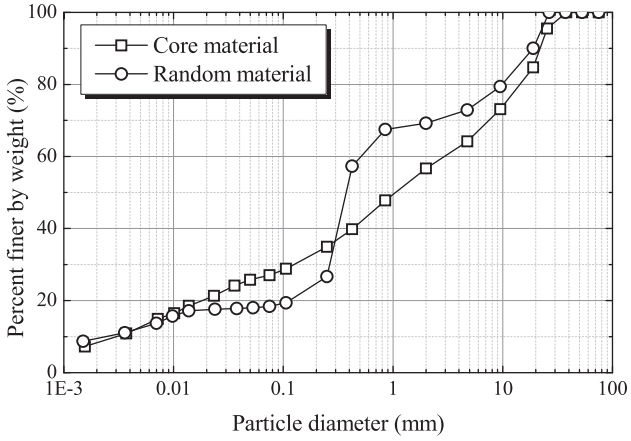

Fig. 2. Grain size cumulative curves.

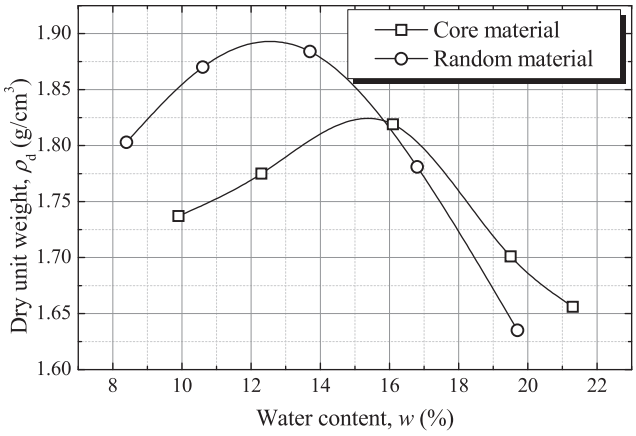

Fig. 3. Compaction curves.

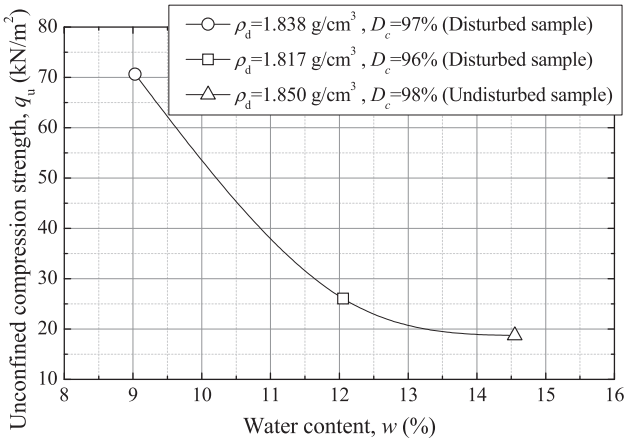

Fig. 4. Relation between water content and unconfined compressive strength.

be different. As a result, it is thought that the permeability coefficient changed by 10 times between the two specimens.

2.4.2. Random material

Except for in the sloping core zone, random fill was used as the embankment material. The random fill consisted of the cohesive soil used for the core and silica sand excavated from a borrow-pit in Kyotango City, Kyoto Prefecture. The silica sand was mixed with the cohesive soil to increase the permeability of the random fill because there was not enough time for seepage after filling the water due to time constraints. It is reasonable to use sandy soils as the random fill for small earth dams. As mentioned earlier, sandy embankments have sustained more damage in past earthquakes than cohesive embankments. Moreover, when repairing embankments using GCLs, sandy soils can be used as embankment fill on the upstream side of the GCLs. Based on the permeability and slope stability during the construction [for details, refer to Sawada et al. (2016)], the mix ratio was approximately 1:1 by volume. According to the Unified Soil Classification System of Japan, the soil is classified as SFG. The properties of the random fill, the grain size cumulative curves, the compaction curves, and the relation between the water content and the unconfined compressive strength are shown in Table 2 and Figs. 2–4, respectively. Fig. 4 shows that the unconfined compressive strength decreases with an increasing water content, which can be attributed to the decline in suction.

Table 2
Properties of the random fill material.

Soil particle density ρ_s (g/cm^3)	2.644
Average diameter D_{50} (mm)	0.37
Uniformity coefficient U_C	185
Coefficient of curvature U_C'	64.1
Optimum water content w_{opt} (%)	12.6
Maximum dry density ρ_{dmax} (g/cm^3)	1.890
Liquid limit w_L (%)	NP
Plastic limit w_P (%)	NP

2.4.3. GCL

The GCL used in the present study was composed of granular bentonite sandwiched between a woven polypropylene geotextile and a nonwoven polypropylene geotextile, which were needle-punched together, as seen in Fig. 5 (Volclay Mat ST, Volclay Japan Co., Ltd.). The frictional properties between the core soil and the GCL have already been examined by Sasaki et al. (2015) using direct shear tests. They found the cohesion and friction angle between the woven and the non-woven GCL components to be 15 kN/m^2 and 28°, respectively. The cohesion and friction angle between the core soil and the woven GCL component were 0 kN/m^2 and 34°, respectively. Under low confining pressures, as in the present study, the interface between the woven GCL component and the core soil might be the weak point of the embankment. However, it should be noted that the frictional properties in this study will be different from those in past studies because the random fill here comes in direct contact with the GCL instead of the core soil.

2.5. Model construction

Prior to the model construction, a test embankment (Sawada et al., 2016) was created to determine the spreading depth and compaction number. To achieve a lift thickness of 0.2 m, spreading depths of 0.25 and 0.23 m were used for the core material and the random fill, respectively. In addition, considering 95% of the maximum dry density

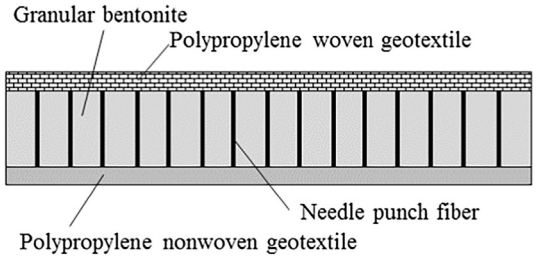

Fig. 5. Schematic of the GCL.

Photo 2. Installation of the GCL (Sawada et al., 2016).

on the basis of the Proctor test described in JIS-A 1210, as prescribed by the current guidelines (Ministry of Agriculture, Forestry and Fisheries, 2015a), the compaction numbers obtained using a vibrating roller (800 kg) and a plate compactor were 6 and 8, respectively.

After the test embankment, the embankment models were built in the containers. The core material and the random fill were mixed with water to obtain the optimum water contents. The mixture was then packed into ton bags and transported into the containers using a rough terrain crane. A compact excavator and rakes were employed for placing and spreading the mixture, and a vibrating roller and plate compactor were employed for compaction. After filling, the extra fill was cut using the compact excavator.

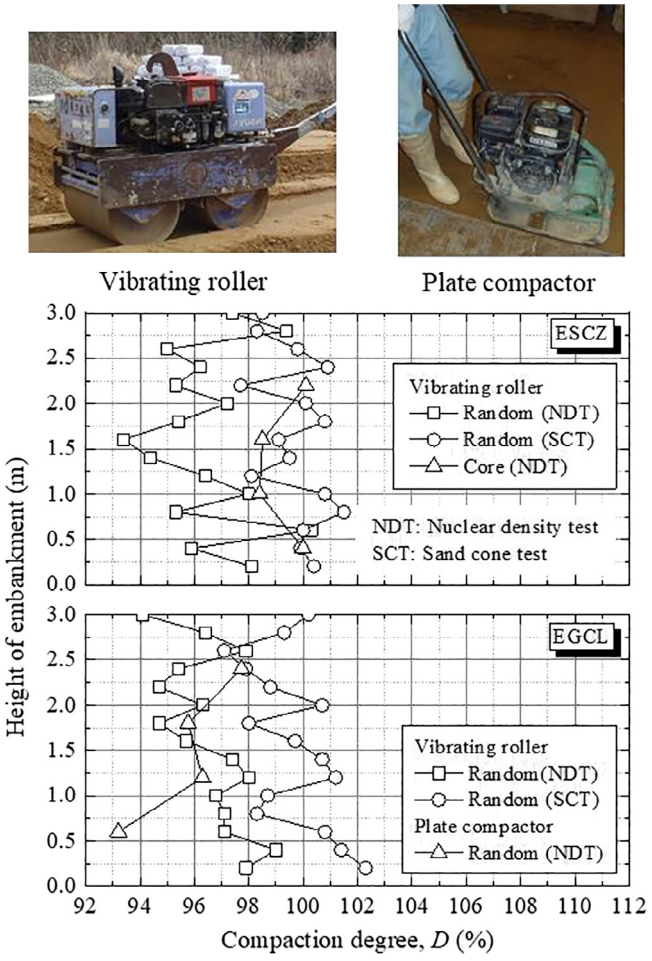

Fig. 6. Compaction degrees of embankments (modified from Sawada et al., 2016).

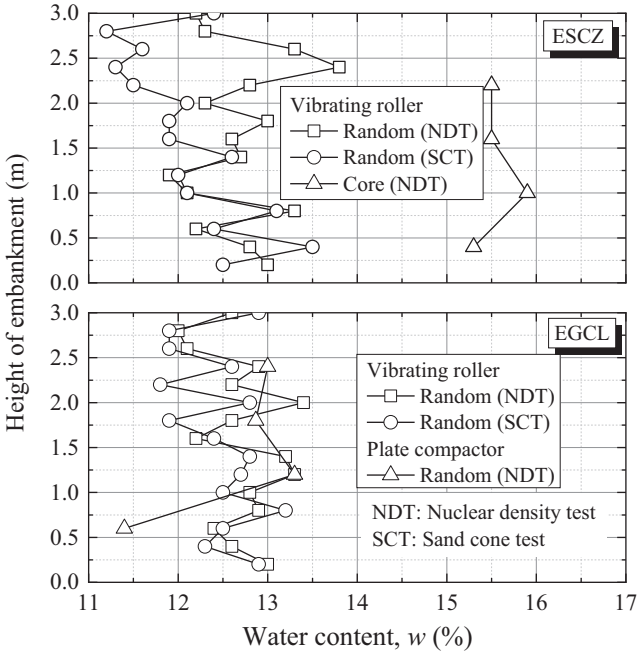

Fig. 7. Water content of embankments.

For the embankment with a GCL, a bench cut with an inter-ramp slope of 1:1.5 was made at the upstream side, and the GCL was set on the bench, as shown in Photo 2. The bottom of the GCL along the bed had a width of 0.7 m, and granular bentonite was spread between the GCL and the bed to prevent leakage. On the upstream side of the GCL, the random fill was spread and compacted eight times using the plate compactor.

The soil density and the water content were measured using the nuclear method and the sand cone method, as shown in Figs. 6 and 7, respectively. For the nuclear method, testing was performed at three locations for the lift thickness of each embankment layer, whereas the sand cone testing was performed at one location for each layer. For the two embankments, the degrees of compaction were at least 93% and more than 95% on average.

2.6. Measurements

Fig. 8 shows the locations of the sensors. The accelerometers (ASW-5AM36, Kyowa Electronic Instruments Co., Ltd.) and pore water pressure transducers (BPR-A-200KPS, Kyowa Electronic Instruments Co., Ltd.) were embedded at the prescribed locations at intervals of 0.6 m and are referred to as "A" and "P," respectively. To measure the displacements of the crest and the slope, laser

displacement sensors (LK-500 and IL-2000, KEYENCE Corporation) were installed after the construction of the embankments. Since the soil behavior near the sloping core zone and near the GCL was expected to be different from that at other locations, the transducers were closely spaced. In order not to reinforce the embankments with sensor cables, 5-mm-diameter cables were used and meandered. Pore water pressure transducers P1-09 and P2-09 were set

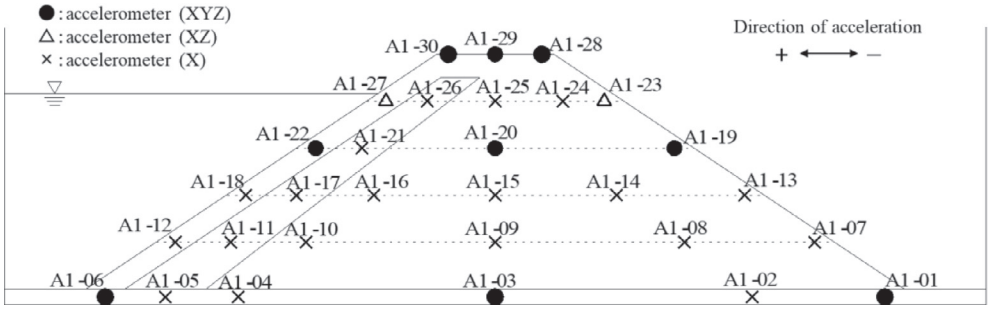

a) Accelerometers (ESCZ)

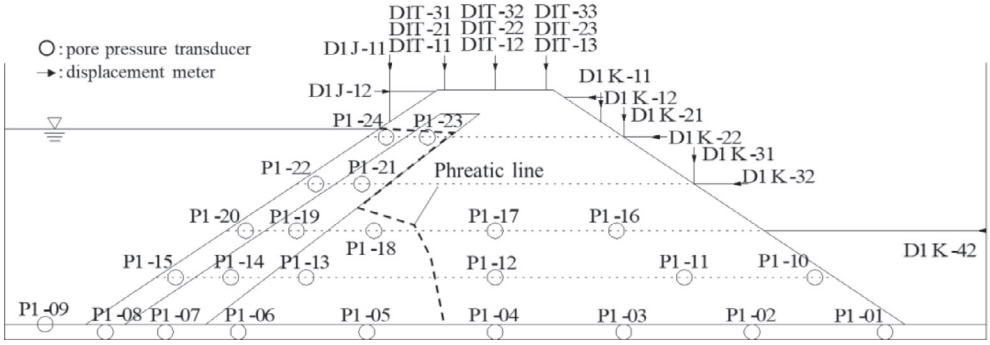

b) Pore pressure transducers and displacement meters (ESCZ)

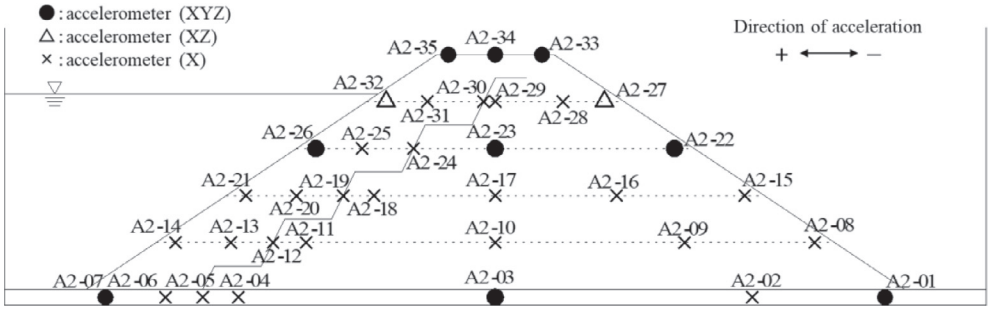

c) Accelerometers (EGCL)

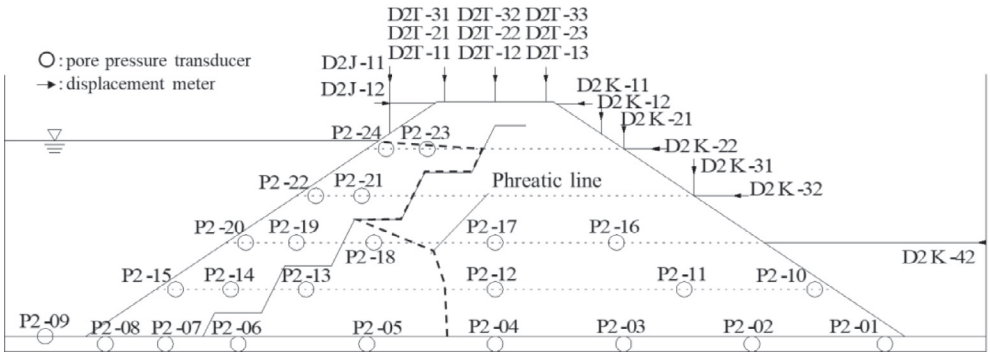

d) Pore pressure transducers and displacement meters (EGCL)

Fig. 8. Sensor locations (modified from Sawada et al., 2016).

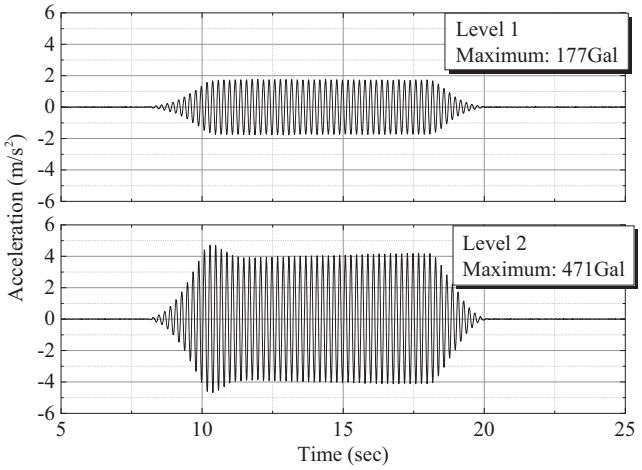

Fig. 9. Base acceleration time histories (Sawada et al., 2016).

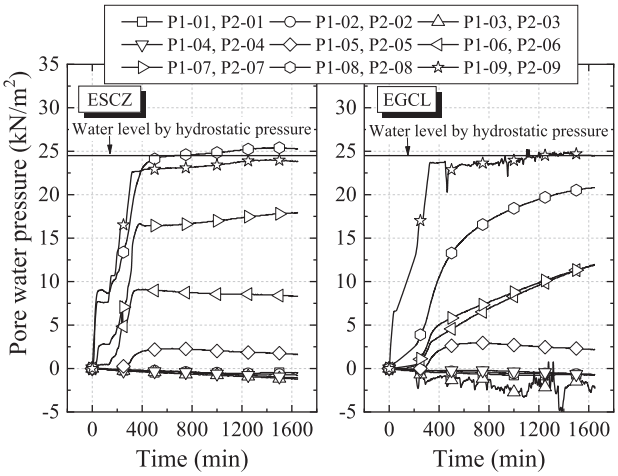

Fig. 10. Pore water pressure in the beds over time (Sawada et al., 2016).

on the bed to measure the water level of the reservoir. Pore water pressure transducers P1-01 to P1-08 and P2-01 to P2-08 were installed −0.1 m from the surface of the bed and backfilled with random fill instead of core material to correctly measure the water head pressure. It should be noted that P2-07 was installed under the GCL and that P2-08 was located on the upstream side.

2.7. Input motion

Simple sine waves in the transverse direction of the embankments were used as the input motion because the purpose of this study was to obtain benchmark data for comparison with the results of numerical analyses, not to simulate earthquake damage in a specific dam. A wave frequency of 5 Hz was chosen in order to avoid the sloshing frequency of water in the reservoir, which was predicted by Housner's equation (Housner, 1963). The wave period was 12 s and had tapered parts (4 s). Two shaking events were designed to reproduce Level-1 and Level-2 seismic motion, as described by the Japanese guidelines (Ministry of Agriculture, Forestry and Fisheries, 2015b); they are hereinafter referred to as Level-1 and Level-2 shaking, respectively. They were subsequently applied to the same model. The base acceleration time histories measured in the two tests are shown in Fig. 9. The peak accelerations of the motions for Level-1 and Level-2 shaking were 177 and 471 Gal, respectively.

3. Results and discussion

3.1. Pore water pressure during pouring

Fig. 10 shows the pore water pressure in the beds over time while water was being poured into the reservoir. P1-09 and P2-09 indicate the hydrostatic pressure, which was equivalent to the water level. The pore water pressure at the base behind the sloping core zone and that near the GCL (P1-06 and P2-06) were much lower than those in front of them (P1-08 and P2-08), which can be attributed to the impervious effects of the protections. Based on all the pore water pressure values, the phreatic lines were determined (Fig. 8). These results clearly show that the soil had been saturated on the upstream side and unsaturated on the downstream side.

3.2. Apparent damage to embankments

After Level-1 shaking, no apparent damage (e.g., cracks or leakage) was observed in either embankment. Conversely, after Level-2 shaking, small cracks with widths of 1 mm and depths of 100 mm were observed in the upstream and downstream slopes of the ESCZ model (Fig. 11), whereas large longitudinal cracks developed at the crest of the embankment in the EGCL model (Fig. 12). Oda et al. (2016) reported mixing water with lime and pouring it into the cracks to investigate their depth. The results revealed that the cracks had developed to the corner of the highest step of the GCL and that the lime had remained along the highest slope of the GCL, as shown in Fig. 12. In addition, according to the article, although the lime was not observed in deeper places, because the cracks were narrow, the acceleration near the GCL indicated that the seismic characteristics were different on the upstream and downstream sides of the GCL. However, no water leakage was observed in either embankment in this study. According to the current guidelines (Ministry of Agriculture, Forestry and Fisheries, 2015a), if a crack occurs in a dam body, the embankment must be repaired. However, the guidelines state that seismic evaluations against Level-2 seismic motion are not done for small earth dams unless the capacity exceeds 100,000 m^3 or the height exceeds 10 m. Based on the degree of damage caused to the embankments by subjecting them to Level-1 and Level-2 shaking, it can be judged that small earth dams with a height of 3 m have earthquake resistance, which is described in the current

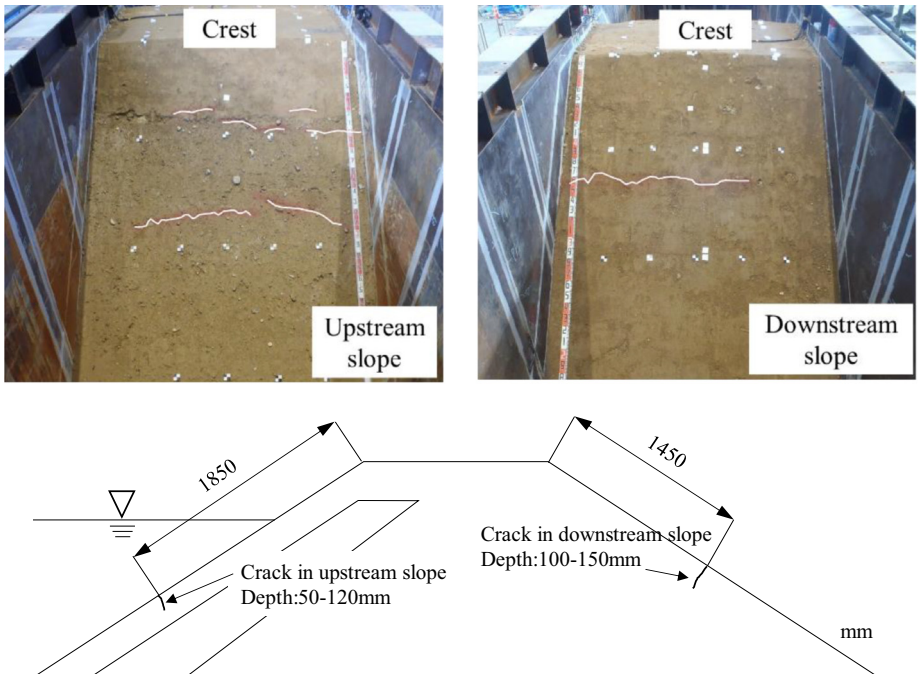

Fig. 11. Cracks in the ESCZ model (modified from Sawada et al., 2016).

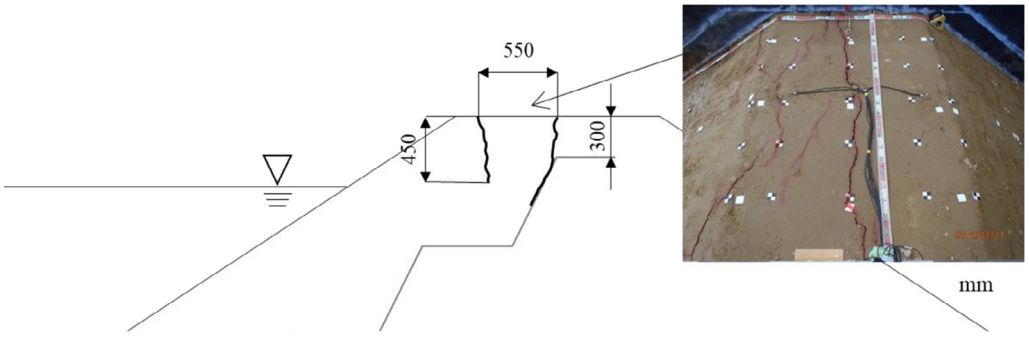

Fig. 12. Cracks in the EGCL model (modified from Oda et al., 2016).

guidelines, if the embankments are sufficiently compacted, such as in the present study.

3.3. Embankment deformation

Figs. 13 and 14 show the time histories of the vertical displacement at the crest of the embankments and the horizontal displacement at the upstream and downstream slopes of the embankments during shaking, respectively. The displacements of the embankments during pouring and after shaking were negligibly small. The positive vertical displacements and the positive horizontal displacements, seen in these figures, were determined as the settlements and displacements in the direction of the upstream side. For both cases, the displacements at the crest and the slope of the embankments during Level-1 shaking were less than 1 mm.

In both cases, the displacements increased gradually from the beginning of Level-2 shaking until the end of shaking. It should be noted that the target plates of sensors D2T-21 and D2J-12 were greatly displaced, and that the distance between the sensors and the targets exceeded the upper limit. Figs. 13 and 14 show that the vertical displacements at the crest and the horizontal displacements at the upper parts of the downstream slopes become positive, whereas the horizontal displacements at the upper parts of the upstream slopes and at the lower parts of the downstream slopes become negative. These results correspond to those of the survey data obtained before and after the tests using electro-optical distance measurements (Fig. 15). It should be noted that the displacements shown in Fig. 15 are enlarged by 10 times. In both embankments, settlement occurred at the crest, and lateral deformation occurred from the middle to the bottom of the embankment.

As shown in Figs. 14 and 15, the amount of settlement was almost of the same degree in both models. Namely, embankments with a GCL are not likely to be inferior to those with a sloping core zone.

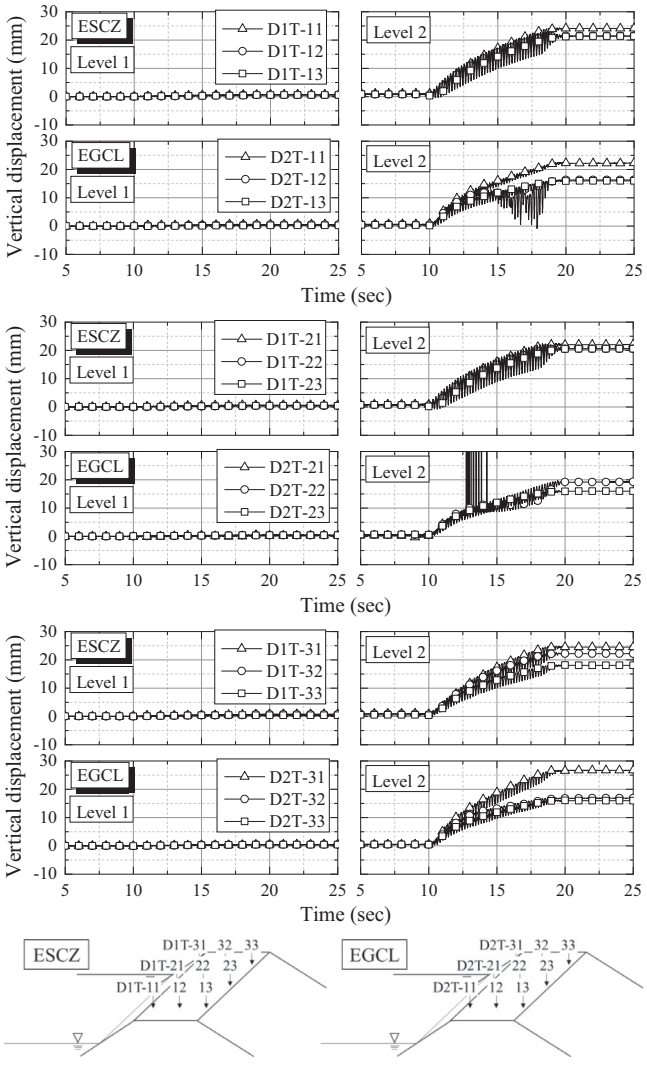

Fig. 13. Time histories of vertical displacement at embankment crests.

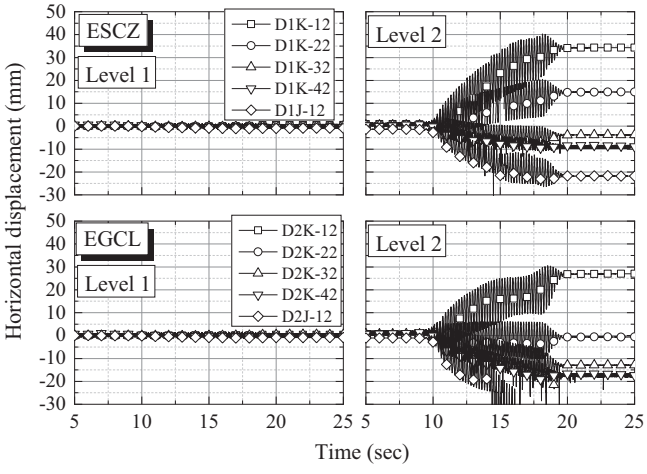

Fig. 14. Time histories of horizontal displacement at embankment slopes.

The settlement on the upstream side was larger than that on the downstream side for two reasons: (1) the increased acceleration was caused by the reduction in shear elastic

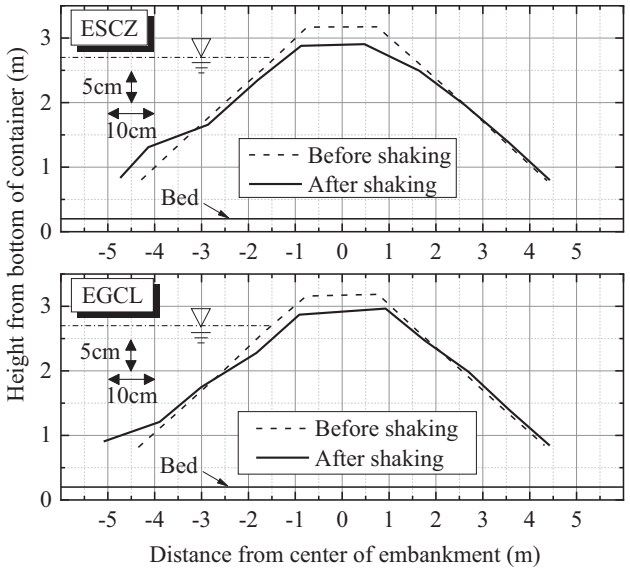

Fig. 15. Cross-sections of embankments before and after shaking (modified from Nakazawa et al., 2017).

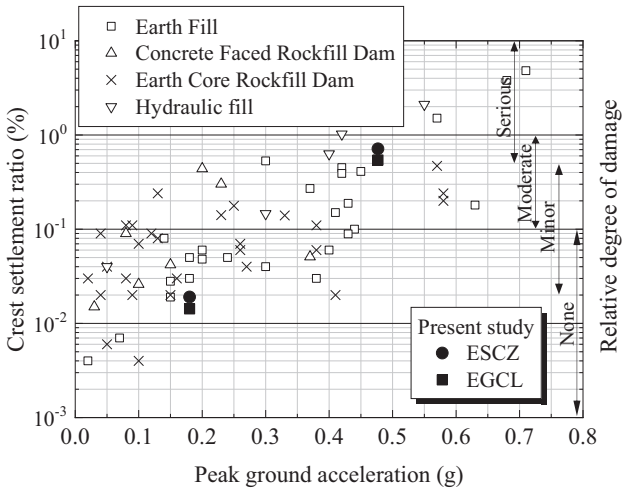

Fig. 16. Relations between peak ground accelerations and crest settlement ratios (modified from Swaisgood, 2003).

stiffness with the increasing water content; and (2) there was a decrease in suction for the saturated soils, as shown in Fig. 4.

The residual crest settlements, which were given as the average values of the nine laser displacement sensors, were 21.4 mm in the ESCZ embankment and 16.7 mm in the EGCL embankment. These settlements are equivalent to 0.71% of the dam height in the ESCZ and 0.54% of the dam height in the EGCL. The ratio of crest settlement to dam height is used as a parameter to quantify the dam damage because the settlement corresponds to the deformation of the dam body, sliding, cracking, and so on (Swaisgood, 2003).

Swaisgood (2003) reviewed and analyzed nearly 70 case histories of dam embankments that had experienced an

earthquake. The article stated that the crest settlement ratio is closely related to the peak ground acceleration and damage severity. Fig. 16 shows the data from Swaisgood (2003) alongside the settlement ratios obtained in this study. Fig. 16 shows that the settlement ratios observed after the Level-1 shaking can be classified as no damage, whereas those observed after the Level-2 shaking are classified as moderate to serious damage. As mentioned above, several large longitudinal cracks were observed at the crest of the EGCL model after the Level-2 shaking. Therefore, it is likely that the deformation behavior observed in our models is reasonable and similar to that occurring in the field during an earthquake.

3.4. Measured accelerations

Figs. 17 and 18 show the measured accelerations for the two embankments during the Level-2 shaking. It should be noted that the scales of the vertical axes for the upstream sides were ± 60 m/s^2, whereas those for the center and downstream sides were ± 20 m/s^2.

At the centers of the embankments, the measured accelerations increased as the location on the embankment became higher. In other words, the input wave was more amplified toward the upper part of the embankment, which is a general dynamic characteristic of elastic solids. The amplification factor between the bed and the crest was

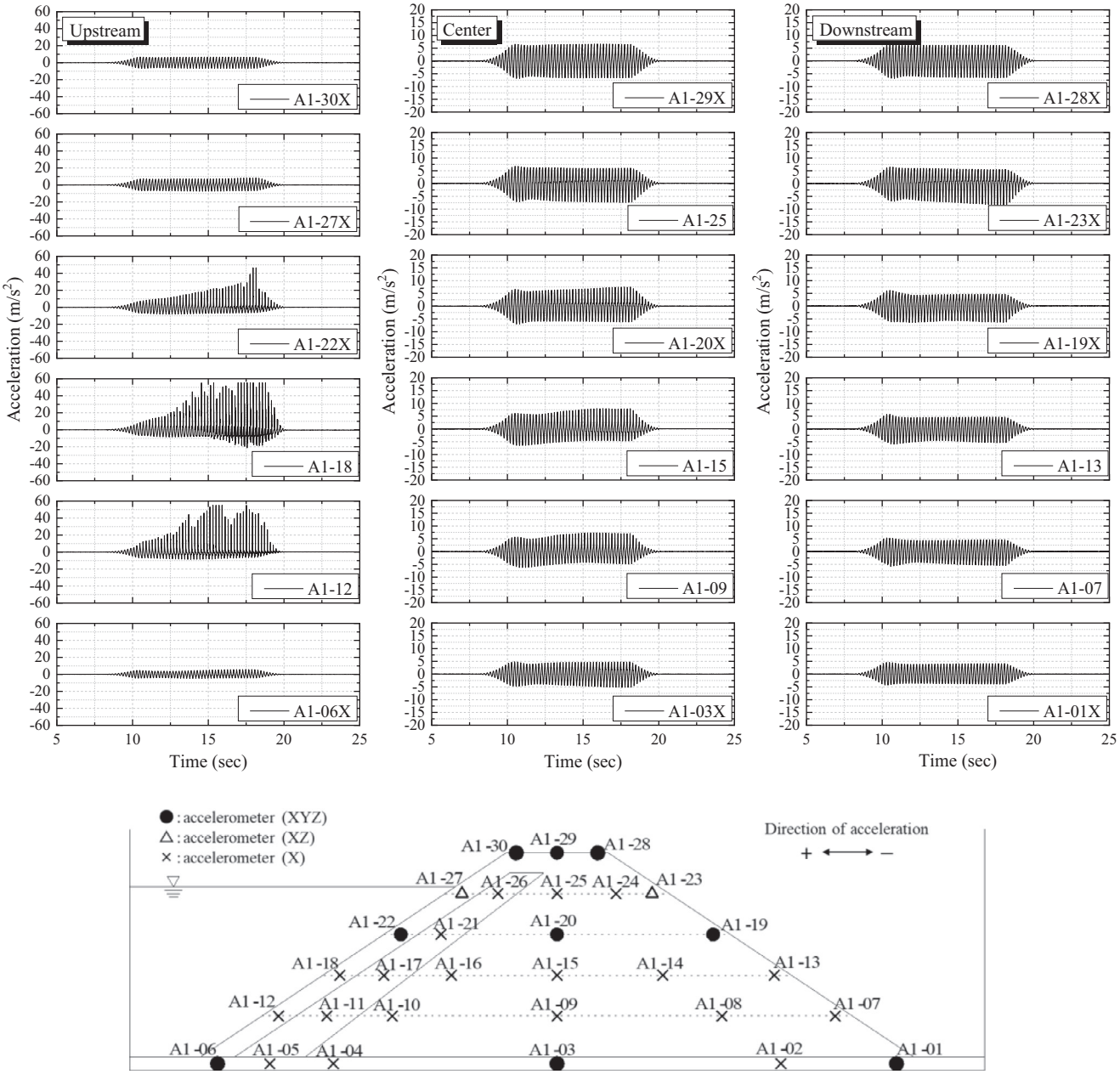

Fig. 17. Measured accelerations (ESCZ).

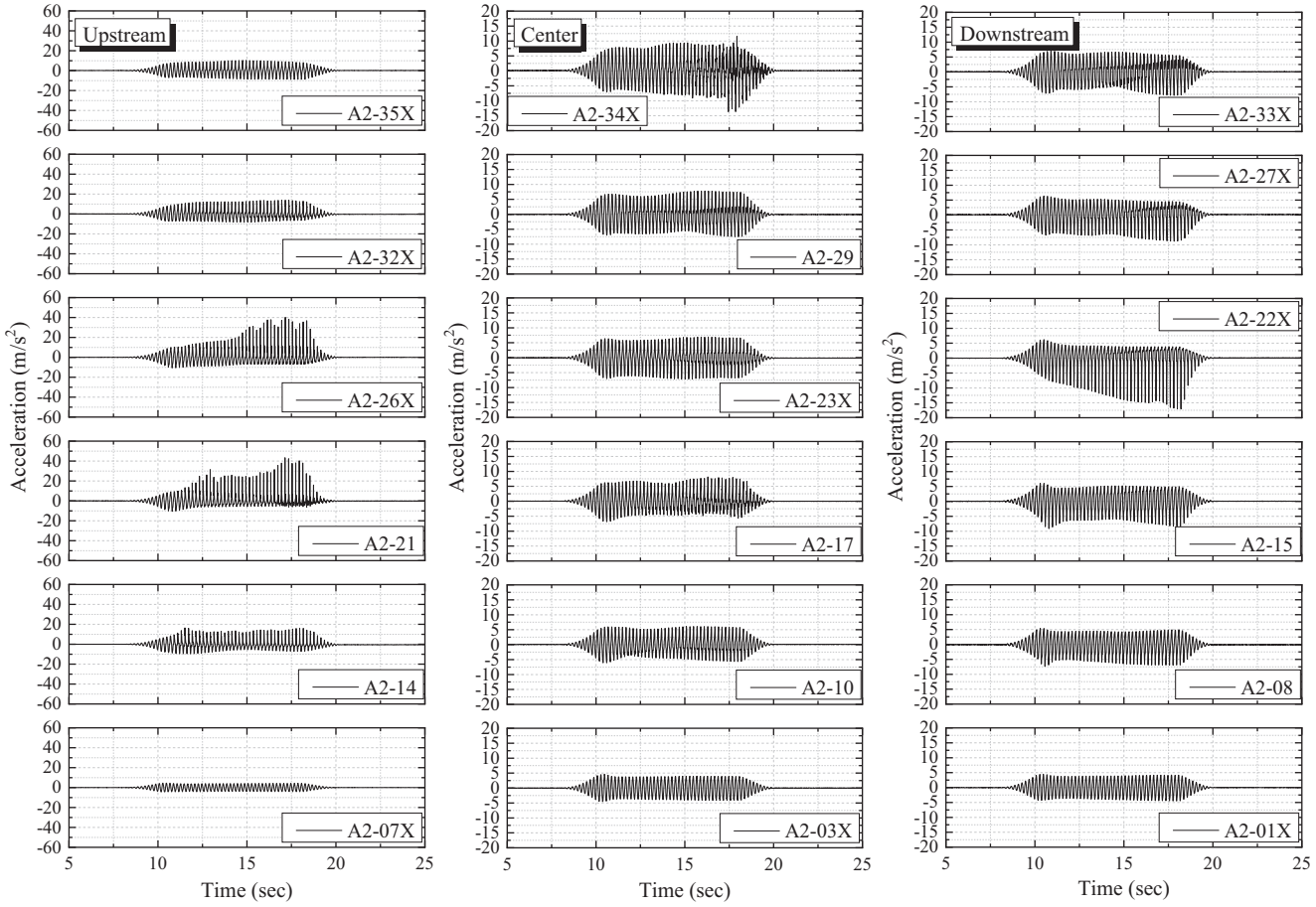

Fig. 18. Measured accelerations (EGCL).

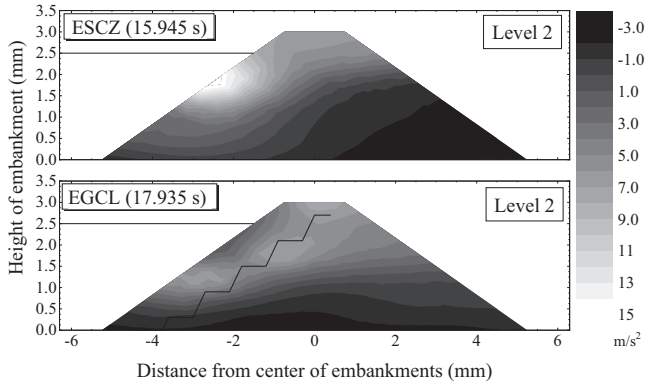

Fig. 19. Distributions of measured accelerations (maximum acceleration at the crest).

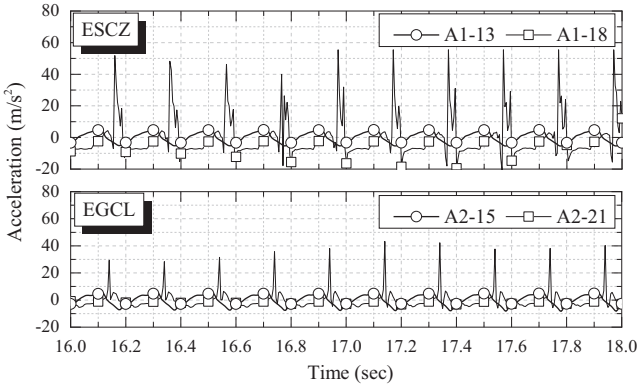

Fig. 20. Measured accelerations from 16 to 18 s.

approximately 1.4 in the ESCZ model. In contrast, in the EGCL model, the amplification factors were 2.1 and 3.3 before and after the development of cracks at the crest, respectively. It appears that the increase in amplification factor was caused by the cracks in the crest. The soil mass on the upstream side was separated from the dam body and moved more freely after the appearance of cracks than before it (i.e., the resistance decreased).

On the upstream and downstream sides, the measured accelerations from the middle to the bottom of the embankments are asymmetric. Namely, the positive amplitude is much larger than the negative one on the upstream side. Conversely, the negative amplitude is much larger than the positive one on the downstream side. These trends are stronger on the upstream side than on the downstream side. According to Higo et al. (2015), this occurs because the shear elastic stiffness decreases with an increasing water content, leading to a smaller impedance ratio. These results agree with the deformation of the embankment, as shown in Fig. 15.

Fig. 19 shows the contours of the measured accelerations when the accelerations at the crests were maximized in the upstream direction (15.945 s in the ESCZ model and 17.935 s in the EGCL model). Fig. 20 shows enlarged views of the measured accelerations on the upstream and downstream sides at the height of 1200 mm above the bed. A large difference in phase was observed between the measured accelerations. In other words, when the upstream slope was displaced toward one side, the downstream slope was displaced toward the other side, most

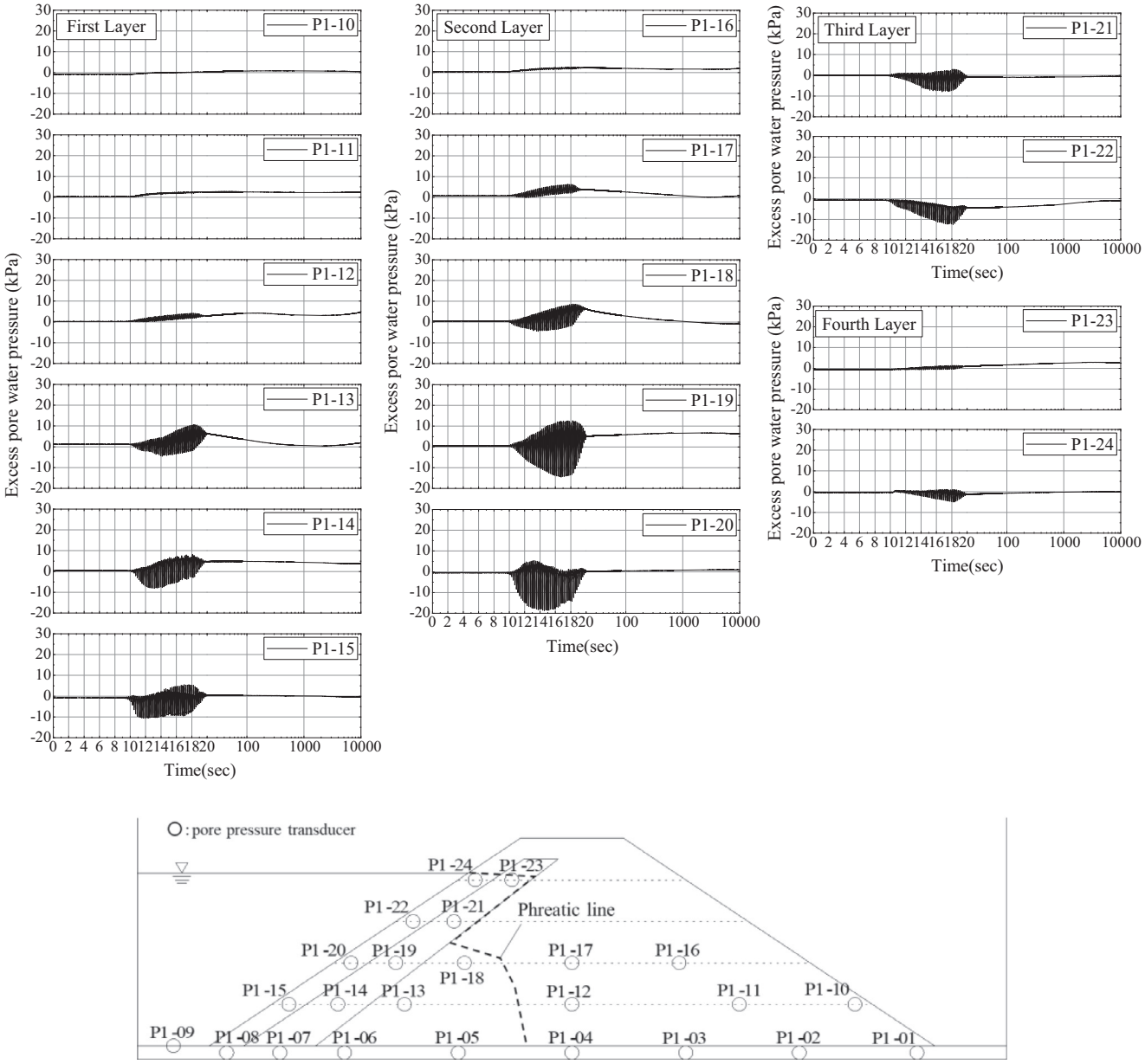

Fig. 21. Time histories of pore water pressure (ESCZ).

likely because the unit weight of the soil on the upstream side is higher than that on the downstream side. This phenomenon may generate tensile stress, potentially damaging rigid concrete structures that are constructed in the transverse direction of the dam bodies (e.g., flood spillways and bottom conduits).

3.5. Response of excess pore water pressure (EPWP) during shaking

Figs. 21 and 22 illustrate the excess pore water pressure (EPWP) over time during Level-2 shaking in both embankment models. In order to discuss the dissipation process of pore water pressure, the x-axes in Figs. 21 and 22 are presented as logarithmic scales after 20 s of shaking.

Regarding the EPWP on the upstream side of the impermeable materials (i.e., the sloping core zone or the GCL), the EPWP hardly accumulated, except for at P1-22 and P2-19. The negative amplitude of the EPWP was much larger than the positive one. The negative pore water pressure is related to the undrained shear behavior of compacted soils; namely, the undrained condition was retained because of the short shaking period (12 s) and no volume change occurred in the soils. This behavior probably led to an increase in effective stress in the saturated soils as well as the restraint of slope failure on the upstream side. Therefore, it is suggested that compaction control by 95% of the maximum dry density, proposed by the guidelines (Ministry of Agriculture, Forestry and Fisheries, 2015a), is significantly effective for improving

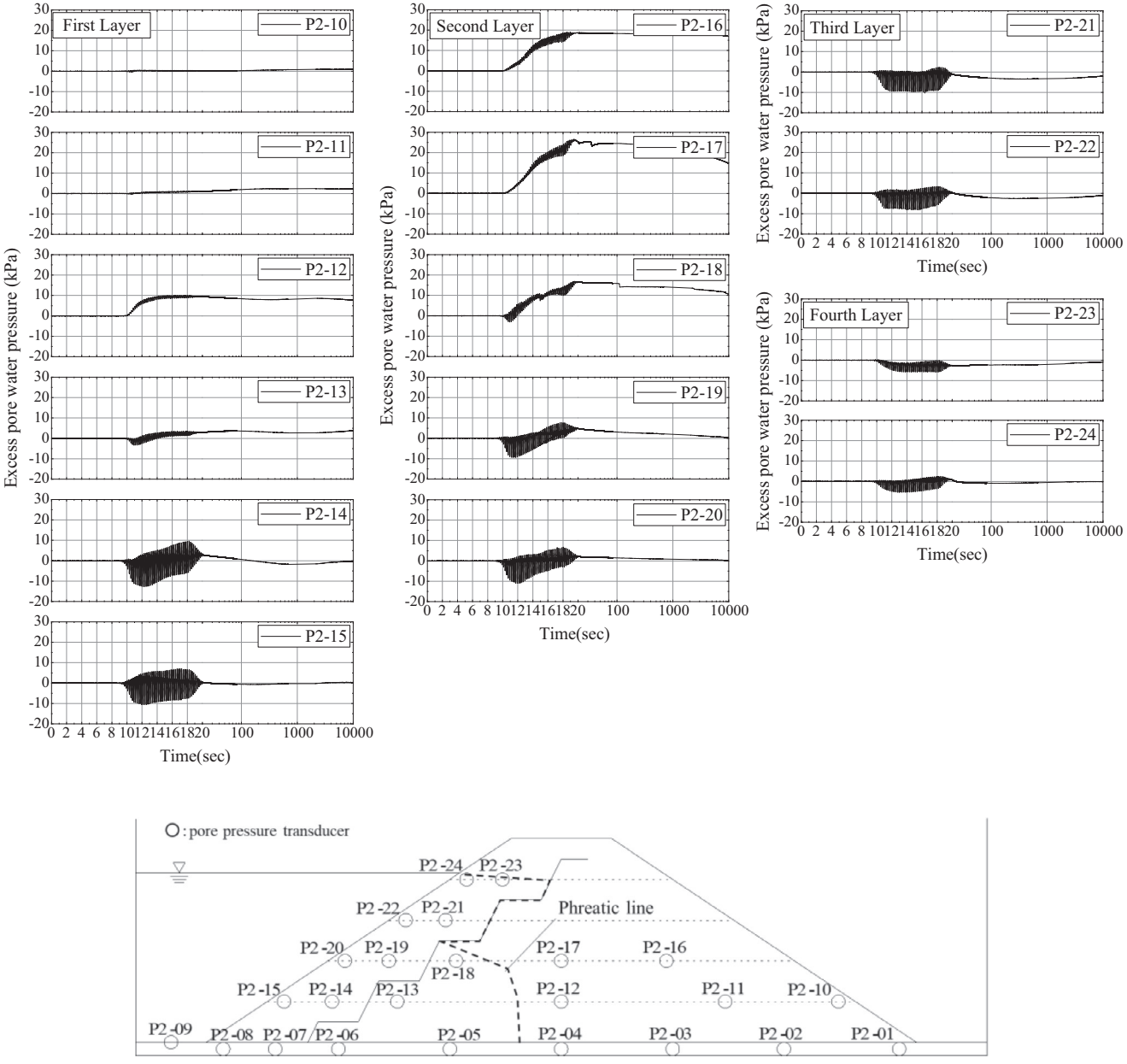

Fig. 22. Time histories of pore water pressure (EGCL).

the earthquake resistance of embankments. However, in the ESCZ model, negative EPWP accumulated in the upper part of the upstream side (P1-22) during shaking and increased gradually after shaking. This probably resulted in volume expansion with water absorption. In other words, the soil became loose and susceptible to liquefaction by subsequent earthquakes. For the EGCL model, the EPWP gradually increased after the decrease in the upper part of the upstream side (P2-21 and P2-22), most likely because of the above-described gap between the GCL and the upstream side. It can be assumed that the pore water around P2-21 and P2-22 flowed into the gap, and that the water was absorbed from the reservoir after shaking.

In the EGCL model, the EPWP at the center and downstream of the embankment increased significantly. Even if a soil is unsaturated, the EPWP increases if the degree of saturation of the soil is relatively high and the negative dilatancy is relatively large. The initial degree of saturation at the center of the third layer (P2-17), determined by a nuclear density test, was 72.6%. The negative dilatancy at P2-17 was expected to be relatively large because the settlement at the crest was approximately 17 mm. The maximum EPWP at P2-17 was 25.7 kPa. The overburden pressure was calculated to be 36.6 kPa using a unit weight of 20.3 kN/m^3 and a depth of 1.8 m. Thus, the maximum EPWP was smaller than the overburden pressure. In the same way, it was found that the EPWP at both P2-16 and P2-18 was smaller than their overburden pressure. Therefore, despite the positive EPWP, this did not appear to be sufficient to cause complete liquefaction. However, liquefaction will occur if a large aftershock strikes within a few hours since their dissipation periods are long.

4. Conclusions

Full-scale shaking table tests using 3-m-high model embankments were carried out to examine the seismic performance of small earth dams repaired by a sloping core zone and a GCL. The embankments were compacted to approximately 95% of the maximum dry density and had reservoirs on the upstream sides. Two input motions of about 170 and 400 Gal were employed to simulate Level-1 and Level-2 seismic motion. The main conclusions of the study are summarized as follows.

Level-1 shaking did not cause water leakage or significant deformation in either embankment model. Conversely, Level-2 shaking produced some cracks in both models, especially in the model using the GCL, and large longitudinal cracks developed at the crest of the embankment with the GCL. In addition to the cracks, deformation also occurred to some extent in both models. The amounts of residual settlements were almost at the same level in both models. Therefore, it can be verified that embankments with a GCL are not inferior to those with a sloping core zone.

Measured accelerations and pore water pressures elucidated the differences in the dynamic behavior on the upstream side and on the downstream side. In terms of the measured accelerations on the upstream side, the positive amplitude was much larger than the negative one because the shear elastic stiffness decreased with an increasing water content. These results agree with the observed embankment deformation. Moreover, a phase difference was seen between the measured accelerations on the upstream and downstream sides. Regarding the changes in pore water pressure at the upstream slopes, the negative amplitude was much larger than the positive one. In other words, the undrained condition was retained because of the short shaking period of only 12 s, and no change in soil volume was generated. This phenomenon probably led to an increase in the effective stress of the saturated soil and prevented slope failure on the upstream side. The findings strongly suggest that the sufficient compaction of upstream embankment material is essential for the earthquake resistance of small earth dams.

Acknowledgements

This work was part of a collaborative research project between Hyogo Prefecture and the National Research Institute for Earth Science and Disaster Resilience and a cooperative research project between Hyogo Prefecture and Kobe University. The Committee for Disaster Mitigation using E-Defense (Director: Tsuneo Okada, Emeritus Professor of Tokyo University) provided helpful suggestions and encouragement. Furthermore, Dr. Kazuo Tani, Professor of Tokyo University of Marine Science and Technology, gave valuable comments and suggestions during the planning of the project. Dr. Satsuki Kataoka, Assistant Professor of Kobe University, provided the test data for the soil materials. The GCL was provided by Volclay Japan Co., Ltd.

References

Aoyama, M., 2011. Rehabilitation of irrigation ponds using bentonite sheets. Water Land Environ. Eng. 79 (8), 44–45 (in Japanese).

Fukushima Prefecture, 2011. Report of the cause of Fujinuma-ike failure <http://www.pref.fukushima.lg.jp/download/1/nosonkeikaku_kensyo_houkoku1-1.pdf> (in Japanese).

Hasegawa, T., Kikusawa, M., 1981. The behavior of a fill-type dam model under dynamic loading by shake table-dynamic characteristics of fill-type dams (I). Trans. Jpn. Soc. Irrig. Drain. Reclam. Eng. 95, 57–64 (in Japanese).

Higo, Y., Lee, C.-W., Doi, T., Kinugawa, T., Kimura, M., Kimoto, S., Oka, F., 2015. Study of dynamic stability of unsaturated embankments with different water contents by centrifugal model tests. Soils Found. 55 (1), 112–126.

Housner, G.W., 1963. The dynamic behavior of water tank. Bull. Seismol. Soc. Am. 53 (2), 381–387.

Hori, T., Ueno, K., Matsushima, K., 2012. Damages of small earth dams induced by the 2011 earthquake of the Pacific Coast of Tohoku. Technical Report in NIRE, 213, pp. 175–199 (in Japanese).

Jeong, K., Shibuya, S., Kataoka, S., Baek, J., Kawabata, T., Sawada, Y., 2016. Seismic behavior and numerical simulation of a small-sized earth-fill with bentonite sheet observed in shaking table test. Jpn. Geotech. Soc. Special Publ. 4 (2), 27–30.

Kawai, T., Ishimaru, M., Noda, T., 2015. Evaluation of seismic behavior of model earth dams in geotechnical centrifuge. Comput. Methods Recent Adv. Geomech., 767–772

Kim, M., Lee, S., Choo, Y., Kim, D., 2011. Seismic behaviors of earth-core and concrete-faced rock-fill dams by dynamic centrifuge tests. Soil Dyn. Earthquake Eng. 31, 1579–1593.

Koyama, A., Suzuki, M., Kochi, Y., Urabe, T., 2014. Deformation behavior of irrigation pond that employs geosynthetic clay liner by shaking table test. Ground Eng. 32, 137–141 (in Japanese).

Ministry of Agriculture, Forestry and Fisheries, 2017. Small earth dam. <http://www.maff.go.jp/j/nousin/bousai/bousai_saigai/b_tameike/> (in Japanese).

Ministry of Agriculture, Forestry and Fisheries, 2015a. Design guideline of land improvement project "Small earth dam" (in Japanese).

Ministry of Agriculture, Forestry and Fisheries, 2015b. Design guideline of land improvement project "Seismic design" (in Japanese).

Mohri, Y., Masukawa, S., Hori, T., Ariyoshi, M., 2014. Damage to agricultural facilities. Soils Found. 54 (4), 588–607.

Nakazawa, H., Sawada, Y., Oda, T., Kobayashi, T., Kobayashi, S., Kawabata, T., Shibuya, S., Kataoka, S., Yamashita, T., 2017. Characteristics on residual deformation of small earth dams in full-scale shaking table tests. J. Jpn. Soc. Civ. Engineers, Ser. A1 (Struct. Eng. Earthquake Eng.) 73, I_815–I_826 (in Japanese).

Oda, T., Sawada, Y., Nakazawa, H., Kobayashi, S., Shibuya, S., Kawabata, T., 2016. Influence of geosynthetics clay liner laid in a staircase shape in embankment on seismic behavior of small earth dam. Geosynth. Eng. J. 31, 175–182 (in Japanese).

Ohne, Y., Tatebe, K., Narita, K., Okumura, T., 1983. Fundamental study on earthquake resistant design of fill-type dams. Trans. Jpn. Soc. Civ. Engineers 339, 127–136 (in Japanese).

Sasaki, T., Kawaguchi, T., Kawajiri, S., Shibuya, S., 2015. Experimental study on friction resistance between soil and bentonite geosynthetic clay liner. Geosynth. Eng. J. 30, 133–140 (in Japanese).

Sawada, Y., Nakazawa, H., Kataoka, S., Kobayashi, S., Oda, T., Kobayashi, T., Shibuya, S., Yamashita, T., Tani, K., Kajiwara, K., Kawabata, T., 2016. Full-scale shaking table tests for small earth dams with sloping core zone and geosynthetic clay lines. Geosynth. Eng. J. 31, 167–174 (in Japanese).

Sendir, S., Sato, J., Towhata, I., Honda, T., 2010. 1-G model tests and hollow cylindrical torsional shear experiments on seismic residual displacements of fill dams from the viewpoint of seismic performance-based design. Soil Dyn. Earthquake Eng. 30, 423–437.

Swaisgood, J.R., 2003. Embankment dam deformations caused by earthquakes. In: Pacific Conference on Earthquake Engineering, Paper no. 014.

Tabata, K., Nakazawa, H., Kajiwara, K., 2017. E-defense improved performance and possible geotechnical model tests on liquefaction behaviors for saturation evaluation. In: 16th World Conference on Earthquake, Paper no. 1492.

Tani, S., 1996. Damage to earth dams. Soils Found. 36, 263–272.

Tani, S., Hasegawa, T., 1987. Earthquake damage on earth dam by The Nipponkai-Chubu Earthquake. J. Jpn. Soc. Agric. Eng. 55 (10), 17–25 (in Japanese).

Yuan, L., Liu, X., Wang, X., Yang, Y., Yang, Z., 2014. Seismic performance of earth-core and concrete-faced rock-fill dams by large-scale shaking table tests. Soil Dyn. Earthquake Eng. 56, 1–12.